Onshore entrapment of sea water in coastal aquifers by rapid coastline progradation

Vaughan R. Voller[1], Adrien Camille[2], Nafis Sazeed[2], Loc Luong[2], Michael S. Steckler[3], Mark Austin Person[2], and Kate Leary[4]

[1]University of Minnesota
[2]New Mexico Tech
[3]Columbia University
[4]New Mexico Institute of Mining and Technology

November 18, 2022

Abstract

We hypothesize that onshore saline groundwater in delta systems may have resulted from rapid shoreline progradation during the Holocene. To explore this hypothesis, we develop a model for the transport of saline groundwater in a shore-normal longitudinal cross-section of an evolving ocean margin. The transport model uses a control volume finite element model (CVFEM), where the mesh of node points evolves with the changing aquifer geometry while enforcing local mass balance around each node. The progradation of the shoreline and evolution of the aquifer geometry is represented by assuming the shoreline advances at a prescribed speed with fixed top and foreset slopes. The combined model of transport and progradation, is used to predict the transient trapping of saline water under an advancing shore-line across a range of realistic settings for shoreline velocity and aquifer hydraulic properties. For homogeneous aquifers, results indicate that the distance behind the shoreline, over which saline water can be detected, is controlled by the ratio of the shoreline prorogation rate to the aquifer velocity and the Peclet number. The presence of confining units probably had the greatest impact in sequestering onshore seawater behind an advancing shoreline. Further support for the validity of the proposed model is provided by fitting model predictions to data from two field sites (Mississippi River and Bengal Deltas); the results illustrate consistent agreement between predicted and observed locations of fossil seawater.

Onshore entrapment of sea water in coastal aquifers by rapid coastline progradation

Vaughan R. Voller[1], Adrien Camille[2], Nafis Sazeed[2], Loc Luong[2], Michael Steckler[3], Mark Person[2], Kate Leary[2]

[1]Department of Civil, Environmental, and Geo- Engineering,

Saint Anthony Falls Laboratory, University of Minnesota,

500 Pillsbury Drive SE, Minneapolis, MN 55455

[2]Department of Earth and Environmental Sciences,

New Mexico Institute of Mining and Technology

801 Leroy Pl, Socorro, NM 87801

[3]Lamont-Doherty Earth Observatory, Columbia University

61 Route 9W, PO Box 1000, Palisades, NY 10964

Key Points:

- We have developed a transient model of the transport of a saline groundwater in an aquifer under a prograding sedimentary delta
- The predicted amount of fossil saline water trapped onshore depends on the ratio of the shoreline advancement to the groundwater velocity
- Our model predictions are consistent with the entrapment of fossil seawater within the Mississippi River and Bengal Deltas

Corresponding author: Vaughan Voller, `volle001@umn.edu`

Abstract

We hypothesize that onshore saline groundwater in delta systems may have resulted from rapid shoreline progradation during the Holocene. To explore this hypothesis, we develop a model for the transport of saline groundwater in a shore-normal longitudinal cross-section of an evolving ocean margin. The transport model uses a control volume finite element model (CVFEM), where the mesh of node points evolves with the changing aquifer geometry while enforcing local mass balance around each node. The progradation of the shoreline and evolution of the aquifer geometry is represented by assuming the shoreline advances at a prescribed speed with fixed top and foreset slopes. The combined model of transport and progradation, is used to predict the transient trapping of saline water under an advancing shore-line across a range of realistic settings for shoreline velocity and aquifer hydraulic properties. For homogeneous aquifers, results indicate that the distance behind the shoreline, over which saline water can be detected, is controlled by the ratio of the shoreline prorogation rate to the aquifer velocity and the Peclet number. The presence of confining units probably had the greatest impact in sequestering onshore seawater behind an advancing shoreline. Further support for the validity of the proposed model is provided by fitting model predictions to data from two field sites (Mississippi River and Bengal Deltas); the results illustrate consistent agreement between predicted and observed locations of fossil seawater.

Plain Language Summary

Saltwater intrusion in coastal aquifers is generally thought to be due to excessive pumping. Here we propose that the rapid advance of the delta front due to lateral sediment transport can entrap seawater onshore. We developed a cross-sectional mathematical model to understand the key controls on onshore seawater entrapment by sediment progradation. Using this model, we found that the ratio of the lateral coastline advance velocity over the groundwater velocity as well as the ratio of advective to dispersive solute transport plays a key role in the extent of seawater capture onshore. Additional analysis showed that the ratio of vertical advective to diffusive transport and the presence of low permeability confining units are also important in the trapping of onshore seawater. We applied our model to the Bengal and Mississippi River deltas using published estimates of shoreline progradation and salinity conditions. Our model is as able to reproduce observed onshore saline water consistent with our hypothesis.

1 Introduction

Over the past several decades, there has been growing concern regarding how onshore groundwater pumping has led to seawater intrusion within coastal aquifer systems (Barlow & Reichard, 2010; Han et al., 2015). More recently, the specter of sea level rise (Chui & Terry, 2013; Lee et al., 2016) and tsunami activity (Violette et al., 2009; K.G. Villholth & Neupane, 2011; Pauw et al., 2012) has also been shown to result in coastal groundwater salinization.

Within the Bengal delta aquifer system, onshore saline groundwater exists within both a deep confined and unconfined aquifer system at depth range between about 40m to 120m and extending 50km onshore (Figure 1a-1b). This onshore seawater appears to be unrelated to any of the above mechanisms. The Bengal Delta has experienced relatively high sediment fluxes resulting in the lateral migration of the coastline ocean-ward by over 100km ave been deposited onshore (Kuehl et al., 2005). As a comparison, the Mississippi delta has a higher aquifer conductivity and thus lower onshore salinities. In the Mississippi River Delta brackish water extends about 60km inland (Figure 1c; Chamberlain et al. 2018).

We hypothesize that rapid deposition of sediments during the Holocene has resulted in entrapment of seawater onshore. In this study, we have developed a coupled sediment transport and groundwater flow/solute transport model to explore under what conditions, seawater can be trapped on shore. Below, we present a sensitivity study that considers different ratios of sediment velocity to hydraulic conductivity that we believe controls the distribution of fossil seawater onshore. We also assess how the hydrodynamic dispersion/diffusion influences onshore seawater sequestration. Finally, We attempt to match field conditions within the Bengal Delta and the Gulf of Mexico using this model as a means of qualitatively providing ground truth for our hypothesis.
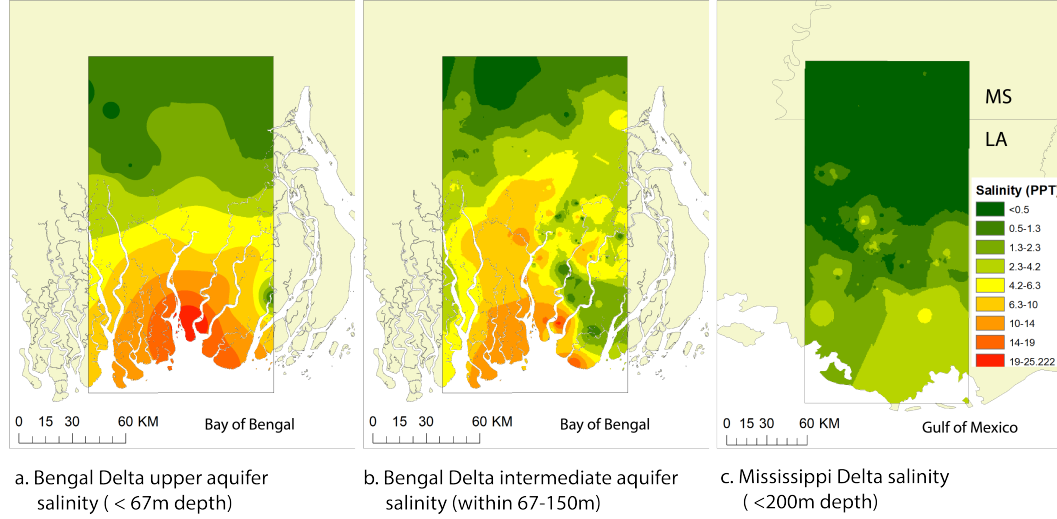

Figure 1. Interpolation maps of Bengal Delta (a & b) and Mississippi River Delta (c) showing planview salinity data (BWDB, 2013).

2 Methods

Below we present the govern transport equations and numerical solution scheme used in this paper.

2.1 Governing Equations

Our governing variable-density groundwater flow equations uses freshwater heads (Post et al., 2007) given by

$$h = \frac{p}{\rho_w g} + y \tag{1}$$

where p [Pa] is pressure, g [m/s^2] is gravity, y [m] is elevation, and ρ_w is the freshwater density (1000 kg/m^3). The governing equation for the conservation of fresh and saline water in an aquifer can be written as (Fahs et al., 2016)

$$S_s \frac{\partial h}{\partial t} = \frac{\partial}{\partial x}\left[K_x\left(\frac{\partial h}{\partial x}\right)\right] + \frac{\partial}{\partial y}\left[K_y\left(\frac{\partial h}{\partial y} + C(\rho_{rel}-1)\right)\right], \tag{2}$$

Here, K_x, K_y [m/s] are the isotropic hydraulic conductivity tensor components (variations with saline concentrations have been neglected), S_s [1/m] is the specific storage, ρ_{rel} [-] is the ratio of the density of saturated saline to fresh water, and C [-] is the salt concentration ($C = 1$ corresponding to the saturated condition). Note we can write eq.

(2) in the condensed form as

$$S_s \frac{\partial h}{\partial t} = \frac{\partial}{\partial x} \left[-q_x \right] + \frac{\partial}{\partial y} \left[-q_y \right], \tag{3}$$

where the discharge components are defined as

$$q_x = -K_x \left(\frac{\partial h}{\partial x} \right), \quad q_y = -K_y \left(\frac{\partial h}{\partial y} + C(\rho_{rel} - 1) \right), \tag{4}$$

The associated governing equation for the conservation of solute (salt) is (Fahs et al., 2016)

$$\phi \frac{\partial C}{\partial t} = \frac{\partial}{\partial x} \left[-q_x C + D_{xx} \left(\frac{\partial C}{\partial x} \right) + D_{xy} \left(\frac{\partial C}{\partial y} \right) \right] \\ + \frac{\partial}{\partial y} \left[-q_y C + D_{xy} \left(\frac{\partial C}{\partial x} \right) + D_{yy} \left(\frac{\partial C}{\partial y} \right) \right], \tag{5}$$

where the dispersion tensor is defined as (Bear, 1972)

$$D_{xx} = \alpha_L \frac{q_x^2}{|\vec{q}\,|} + \alpha_T \frac{q_y^2}{|\vec{q}\,|} + \phi D_{mol}, \tag{6a}$$

$$D_{yy} = \alpha_T \frac{q_x^2}{|\vec{q}\,|} + \alpha_L \frac{q_y^2}{|\vec{q}\,|} + \phi D_{mol}, \tag{6b}$$

$$D_{xy} = (\alpha_L - \alpha_T) \frac{q_x q_y}{|\vec{q}\,|}, \tag{6c}$$

ϕ is porosity, α_L and α_T [1/m] are the longitudinal and transverse dispersivity coefficients, and D_{mol} [m^2/s] is the molecular diffusion of salt in water. Again, on defining the solute fluxes as

$$q_x^C = q_x C - D_{xx} \left(\frac{\partial C}{\partial x} \right) - D_{xy} \left(\frac{\partial C}{\partial y} \right) \tag{7a}$$

$$q_y^C = q_y C - D_{xy} \left(\frac{\partial C}{\partial x} \right) - D_{yy} \left(\frac{\partial C}{\partial y} \right) \tag{7b}$$

we can write this conservation equation in the condensed form as

$$\phi \frac{\partial C}{\partial t} = \frac{\partial}{\partial x} \left[-q_x^C \right] + \frac{\partial}{\partial y} \left[-q_y^C \right], \tag{8}$$

2.2 The solution domain

Figure 2 shows the finite element mesh and solution domain for our model. At a given time $t > 0$, the aquifer domain consists of land and sea-bed components, comprising a subaerial, fluvial topset and submarine foreset and seafloor. The elevations of the seafloor (B) and sea-level (SL) are assumed constant. If the water table is at or close to the land surface, the boundary condition on of this domain are as follows

- The domain bottom and sides are no-flow boundaries.
- On the topset ($\eta(x) \geq SL$) the solute concentration is set to $C = 0$ and the head is set as $h = \eta(x)$, where $\eta(x)$ is the current land surface elevation at seaward distance $0 \leq x \leq L$.
- On the seabed (foreset and seafloor, $\eta(x) < SL$) the solute concentration is set to the seawater concentration, $C = 1$ and the head is set to the equivalent freshwater value $h = \eta(x) + (SL - \eta(x))\rho_{rel}$, where $\eta(x)$ is now the elevation of the seabed.
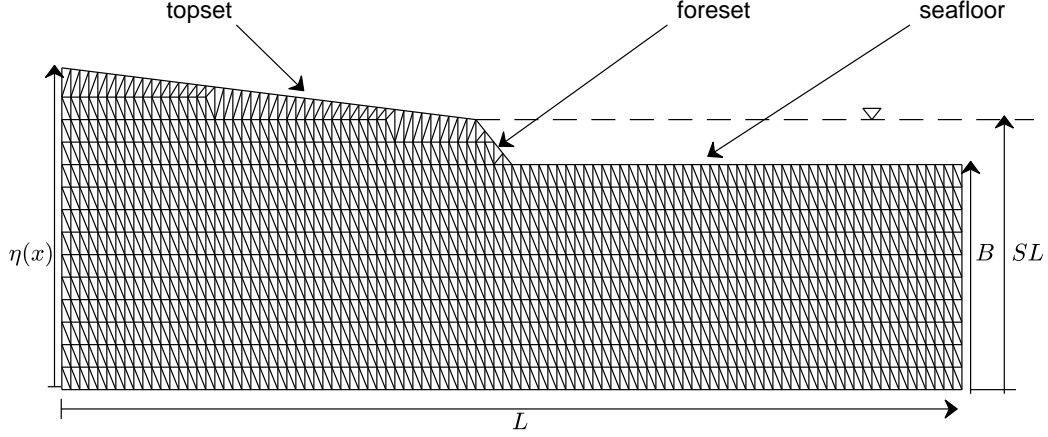
Figure 2. The solution domain and finite element discretization, at time $t > 0$. (Height to Length aspect ratio is 25).

A key part of the proposed model is that the domain evolves through time. At the initial time, $t = 0$, the highest point in the domain is at the sea-level (see top left schematic in Fig. 3), comprising just the submerged foreset and seafloor. At this initial time, the following conditions are imposed:

- The shoreline (beach) is at $x = 0$.
- The toe of the foreset (the point of intersection between the foreset and seafloor is at $x_{toe} = (SL - B)/S_f$, where S_f is the slope of the foreset.
- The entire aquifer contains fully saturated saline water, $C = 1$ (seawater.

On appealing to the successful models of sedimentary basin evolution, based on purely geometric constructs (e.g., see Voller et al., 2020; Reynolds et al., 1991; Kim et al., 2006; Lorenzo-Trueba et al., 2009), we evolve the domain in time, by assuming that the fluvial topset S_t and foreset S_f slopes retain constant values. Then, by simply translating the toe of the foreset at a prescribed seaward velocity (v_{toe}), we can produce a physically realistic model for the advance of a shoreline, with a characteristic clinoform, over an ocean seafloor, see schematics in Fig. 3.

2.3 Control Volume Finite Element Model (CVFEM)

At a given time step $t > 0$, a mesh of linear triangular finite elements are used to discretize the domain. Each element e is associated with three linear shape functions, $N_i^e(x, y)$, $i = 1, 2, 3$ (Zienkiewicz et al., 2005), each function taking a value of unity at a specified vertex (node=1,2,3) and linearly reducing to zero on the element side opposite the node. In this way, we can provide a linear approximation for a dependent variable $u = h$ or C, over the element e, as

$$u^e(x, y) = N_1 u_1 + N_2 u_2 + N_3 u_3 \tag{9}$$

To move forward with the approximation afforded by the finite element discretization we note that our governing head eq.(3) and concentration eq.(8) equations can be written in the generic form

$$\mu \frac{\partial u}{\partial t} = \frac{\partial}{\partial x} \left[-q_x^u \right] + \frac{\partial}{\partial y} \left[-q_y^u \right], \tag{10}$$
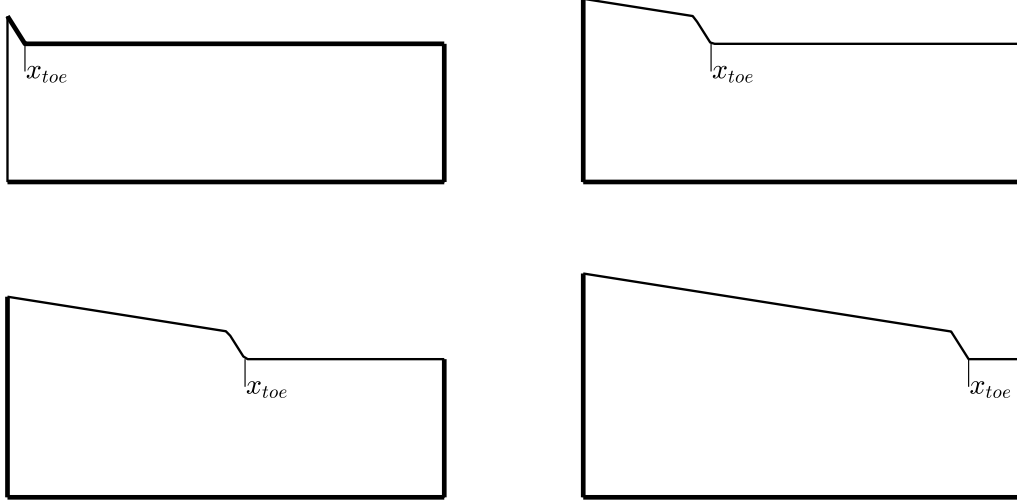
Figure 3. Schematic diagram denoting the model geometry changes in time. The initial domain (top left) only involves the submarine foreset and seafloor. As time increase, the toe (the intersection of the foreset with the seafloor) advances with a prescribed velocity, leading to the appearance of a subaerial topslope. This geomorphology develops in time, under the conditions of constant top- and fore- set slopes, until the model termination (bottom right) when the toe is 95% across the domain L.

For the head calculation, $u = h$, $\mu = S_s$, and the the flux components q_x^u and q_y^u are defined by eq.(4), in the concentration calculation $u = C$, $\mu = \phi$, and the flux components are defined by eq.(7).

On integrating the generic conservation equation, over a closed fixed control volume Ω, with surface Γ, followed by an application of the divergence theorem we arrive at

$$\frac{d}{dt} \int_\Omega \mu u \ dV = - \int_\Gamma q_x^u n_x + q_y^u n_y \ dS \tag{11}$$

where $n = (n_x, n_y)$ is the outward pointing normal on Γ.

The key construction in the Control Volume Finite Element Method (CVFEM) is to add an additional component to the mesh. By joining the mid point of each element to the mid point of each element side, see Fig. 4, we create a tessellation of closed control volumes around each node (element vertex) in the domain. We can associated each of these control volumes with the control volume of the integral equation in eq.(11). Then, following the detail in (Voller, 2009), we can used the geometric properties of the elements and the finite element approximations eq.(9), to numerical approximate the integrals in eq.(11) in terms of the nodal values of the dependent variables. This step produces the following point-wise, time implicit, update, for each node i in the domain mesh

$$\mu V_i u_i = \mu V_i^{old} u_i^{old} + \Delta t \left[\sum_{j=nb} a_j u_j - a_i u_i \right] \tag{12}$$

where V_i is the volume (area) of the control volume, the superscript *old* refers to the previous time step value, the summation is over the neighboring nodes to i, i.e, the nodes that share a common element edge with node i, the a's are known coefficients, and Δt is the time step. In arriving at the coefficients for the concentration equation ($u = C$)

119 an upwind approximation is used (Patankar, 1980), i.e., the concentration in the advec-
120 tive contribution is associated with the nodal value of the control volume from which the
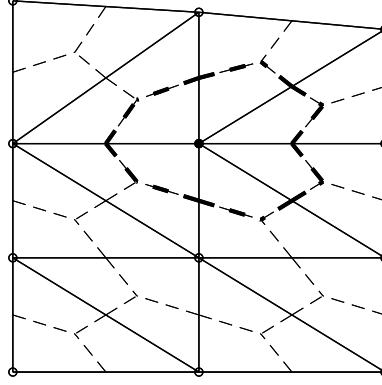121 discharge emerges.

Figure 4. A section of the mesh showing nodes (circles) ,finite elements (sold lines) and con-
trol volumes (dashed lines). The control volume associated with node denoted by the filled circle
is shown as a bolded dashed line.

122 The derivation of discrete update in eq.(12), naturally accounts for no flow bound-
123 aries. At fixed value domain boundary nodes, the update is replaced by an update that
124 imposes the required value for u_i. Each node i on the the domain boundary, has a con-
125 trol volume surface area, A_{bi}, coincident with the domain boundary. In this way, at a
126 node i on a domain boundary with a prescribed water flux, q_{in} [m^3/s], the additional
127 contribution $\Delta t q_{in} A_{bi}$ is added to right-hand side of eq.(12) when updating the head.

128 A separate equation in the form of eq.(12) is solved for both the head and the con-
129 centration. In a time step, the head is updated and groundwater discharges determined,
130 before solving for the concentrations. In the head update, the q_y discharge component
131 (see second term of eq.(4)) is evaluated using the previous time values of C. A point-
132 wise Jacobi iterative scheme is used in the update; a scheme well suited for vectoriza-
133 tion and one that avoids the directional ('skewing') errors that can be induced with Gauss-
134 Seidel iteration. Convergence is declared when the largest value of $|u_i = u_i^{old}|$, $i = 1, 2, \ldots N$
135 (total nodes in the domain), between iterations, falls below a prescribed tolerance *tol* $\sim$
136 $10^{-8} - -10^{-6}$.

2.4 Mesh evolution and motion

138 In our calculations, to account for the evolving shoreline, the finite element mesh
139 changes with each time step, a schematic of the evolution of the mesh is shown in Fig.
140 5. In the mesh there is a fixed number n_{cols} of vertical grid lines (columns), at equally
141 spaced locations $x_j = j\Delta x$, $j = 0, 1, \ldots n_{cols}$, where $\Delta x = L/(n_{cols} - 1)$. Within each
142 time step, starting from the bottom of each column, node points are arranged with a fixed
143 vertical spacing Δ, at locations $y_i = i\Delta$, $i = 0, 1, \ldots top-1$. The fixed spacing is over-
144 ridden, in placing the last node with index *top*. This node, assuming a purely deposit-
145 ing system, tracks the movement of the land/seabed surface, i.e., $y_{top} = \eta(x_j, t)$. To
146 reduce grid distortion, at the point where the spacing between the top node in a column
147 and the node blow, exceeds 1.5Δ, i.e., $y(t)_{top} - top\Delta > 1.5\Delta$, the node index of the
148 top node is advanced $top^{new} = top+1$ and a new fixed position node, with index $ins =$
149 *top*, is inserted on the column, at position $y_{ins} = ins\Delta$. Values of the dependent vari-

ables h_{ins} and C_{ins} at the inserted node are found by linear interpolation between the values at nodes *top* and *ins* − 1.

We note that, the advance of the top surface nodes in each column and, when required, the addition of the new nodes below the advancing surface, will cause the control volumes associated with top surface nodes to change shape and size within a time step, Fig. 5. To simplify the calculation, we assume, that any conserved quantity added or subtracted, as a result of changes in control volume size, does not change the average value in the control volume. Essentially, this means that we can associate previous time nodal values with the current time control volume, i.e., in our iterative scheme, eq.(12), we can set $V_i^{old} = V_i$. We expect that any limitations in this approximation will be exposed in a mesh size /time step dependence study.
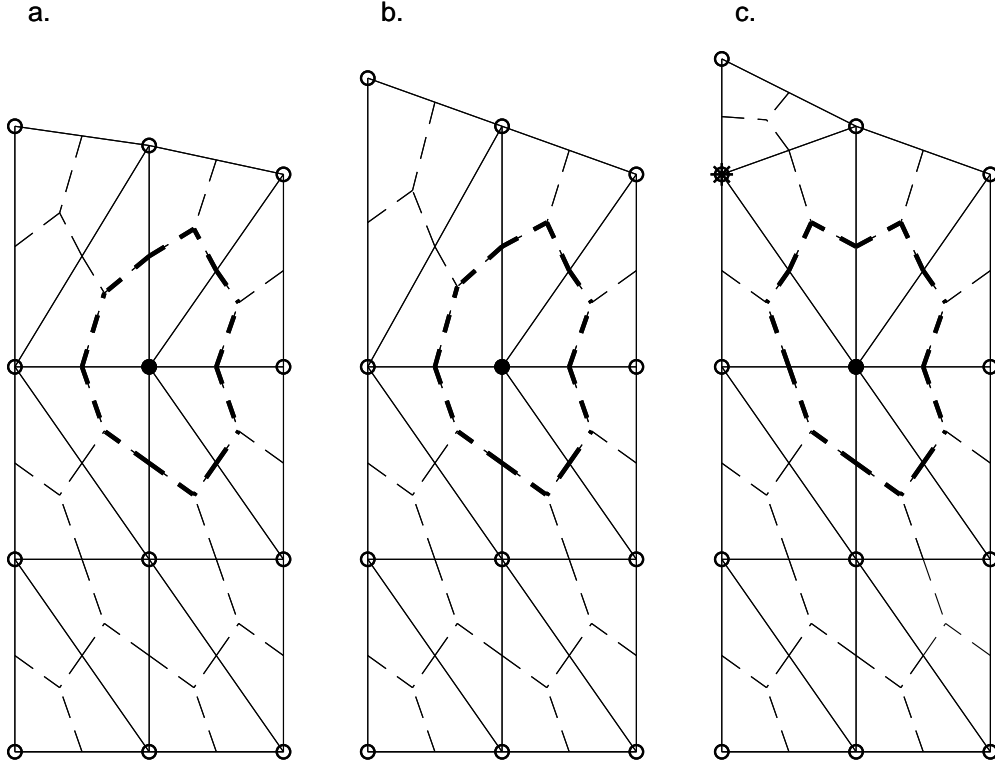

Figure 5. Mesh motion. a. The non-top nodes in each mesh column have fixed location and spacing Δ. b. The top nodes move with the land/sea-bed surface If a top node reaches a vertical position that is more than 1.5Δ above the node below a new node (indicated by the asterisk) is inserted to maintain the Δ spacing.

2.5 Code verification

The code was verified by repeating 'Test Case 2' in (Fahs et al., 2016), where a semi-analytical steady-state solution for the Henry problem is presented. The two-dimensional rectangular problem domain is 1x3(L)m. The physical properties of the aquifer are α_L =0.1 m, α_T=0.01 m, D_{mol}=9.43 10^{-8} m^2/s, $K_x = K_y = 0.01$ m/s, $\rho_{rel} = 1.025$, $\phi = 0.25$, and $S_s = 0$ m^{-1}. The boundary conditions for the head are, top and bottom no flow boundaries, a fixed fresh water flux $q_{in} = 6.6\ 10^{-5}$ m^3/m^2-s on the left, and an equivalent fresh water head $h = y+(1-y)\rho_{rel}$ on the right. The boundary conditions

169 on the solute are, no flow boundaries, top and bottom, and fixed concentration values
170 on the left ($C = 0$) and right ($C = 1$).

171   The linear finite element mesh is created through a Delaunay triangulation on a
172 grid of 81×241 equally spaced nodes. To approach steady state, 60,000 time steps of
173 0.5 seconds are used, a tolerance of $tol = 10^{-8}$ is used to determine convergence.

174   Figure 6 shows plots for steady state predictions for the 10%, 50%, and 90% con-
175 tours of salt concentration. The 50% contour is directly compared (at $y = 0.2, 0.4, 0.6, 0.8$,
176 and 1) with steady state values abstracted from Fig. 5 in (Fahs et al., 2016).
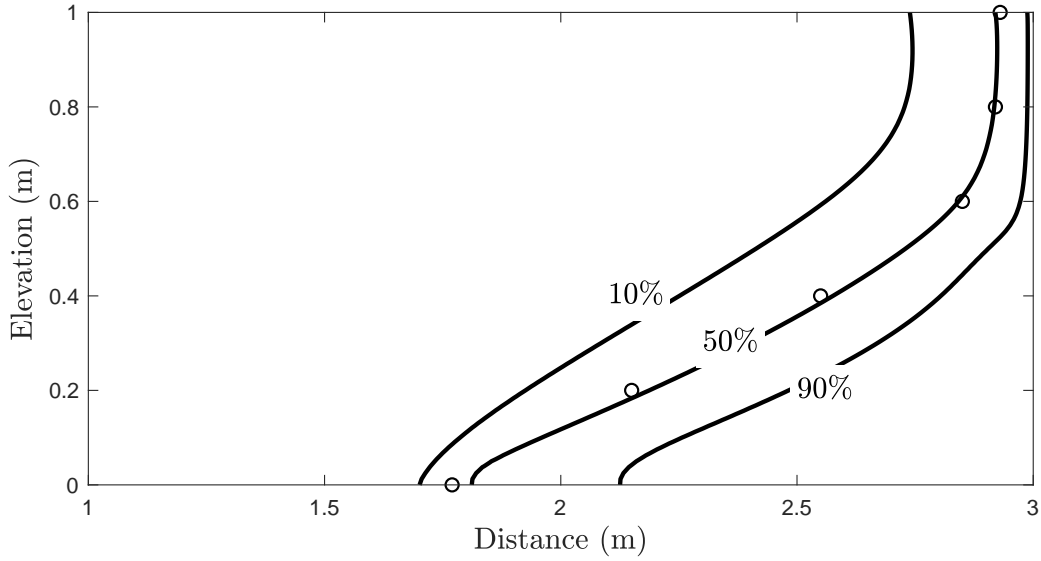

Figure 6.   Predictions of contours of salt concentration. The open circles are values for the
50% contour abstracted from the semi-analytical solution in Fig. 5 of (Fahs et al., 2016). Note.
the scale of this verification test problem 1×3 m, is much smaller than typical field scales

2.6 Model simplifications

178   The main purposes of our model is to demonstrated that saline water can be trapped
179 under the land mass as the shoreline progrades and to identify the key system param-
180 eters that control the level of seawater trapping. Our basic model for this demonstra-
181 tion assumes a simplified constant slope geometry for the domain, a homogeneous aquifer
182 material with constant conductivity, porosity, and storage, and a fixed relative sea-level
183 change. We recognize that relaxing these settings in our model will affect the details of
184 our predictions but expect that they will not undermine the observed general behavior.
185 Thus, we posit that the simplifications in our basic treatment are appropriate for the mod-
186 eling task at hand, broad prediction of the pattern of saline water as a shoreline advances.
187 Note, however, following presentation of results with our basic model we do make ad-
188 ditional runs where we consider confining units—rectangular regions in the aquifer with
189 different conductivity and porosity values.

2.7 Dimensionless groups controlling onshore seawater entrapment

Here we present some heuristic arguments toward identifying the dimensionless groups that control the level of aquifer seawater trapping under a shoreline advances. We have identified two process that control seawater trapping.

The first process is the competition between the rate of advance of the shoreline, dimensions $[\mathrm{LT}^{-1}]$, and the flow velocity of the freshwater recharge $[\mathrm{LT}^{-1}]$. If the shoreline advance is more rapid than the lateral groundwater velocity we should expect the seawater trapping to increase. In our geometric sedimentation model, the rate of the shore line advance is directly given by the prescribed foreset toe velocity v_{toe}. On noting that the driving head gradient, for onshore groundwater flow, is the fluvial topslope, we can characterize the flow velocity of the freshwater recharge as $K_x S_t / \phi$. In this way we see that dimensionless group

$$G_v = \frac{v_{toe}\phi}{K_x S_t} \tag{13}$$

accounts for the competition between shoreline toe advance and freshwater recharge; when G_v is large we expect the shoreline advance to outrun the recharge and promote seawater trapping.

The second process that controls seawater trapping is the level of mixing between fresh and saline water. Typically, in advection-dispersion systems, mixing is controlled by a Peclet number. We can construct an appropriate Peclet number for our system by considering the ratio of the product of a length scale [L] and a characteristic discharge value $\tilde{q}$ $[\mathrm{LT}^{-1}]$, to a characteristic dispersivity $\tilde{D}$ $[\mathrm{L}^2\ \mathrm{T}^{-1}]$. In our system, choosing the length scale as the system depth SL and setting the characteristic dispersivity as $\tilde{D} = \alpha_L \tilde{q}$, arrives at the Peclet number

$$P_e = \frac{SL\tilde{q}}{\alpha_L \tilde{q}} = G_m = \frac{SL}{\alpha_L} \tag{14}$$

When the group G_m is large we would expect the mixing between fresh and salt water to be reduced, leading to an increase in seawater trapping.

So taken together, we propose that the effects of shoreline velocity to recharge and mixing, on seawater trapping is controlled by the dimensionless group

$$G_T = G_v G_m = \left[\frac{v_{toe}\phi}{K_x S_t}\right]\left[\frac{SL}{\alpha_L}\right] \tag{15}$$

3 Results

In order to explore the effects of changing hydrogeologic properties and solute mixing, we conducted a sensitivity analysis in which we varied the hydraulic conductivity of the sediments and the longitudinal/transverse dispersivity (Table 1). Because the water table gradient is fixed by the landward topographic slope, hydraulic conductivity serves as a proxy for groundwater velocity. Simulation parameters that were not varied in the sensitivity study are listed in Table 2. In three simulations (8-10), we included a relatively low-permeability, semi-confining unit 100m thick.

For all model runs, we used a domain 300km in length with 101 nodal columns spaced 3 km apart and a maximum sediment thickness of 400 m. The vertical nodal spacing used was 37.5m. The model was run for 16,370 years using a fixed time step size of 100 days. Over the simulation, the shoreline migrated about 220km. At the end of the simulation, the grid was composed of 1017 nodes and 1195 elements. We present ten simulations in our sensitivity study. One simulation (run 1) we termed the "base case" (Table 1). This simulation used a hydraulic conductivity (K_x) of 5 m/day and a longitudinal dispersivity (α_L) of 50m. Figure 6 depicts changes in salinity through time for the base case. Note

Table 1.   Parameters varied in sensitivity study.

Run	Aquifer Kx (m/day)	α_L	G_T	Confining Unit Kx (m/day)	Figure
1	5	50	33.6	-	6-14
2	10	50	16.8	-	10-11
3	50	50	3.36	-	10-11
4	150	50	1.12	-	10-11
5	5	40	42	-	8-9
6	5	30	56	-	8-9
7	5	20	84	-	8-9
8	5	40	21	0.5	12-14
9	5	30	14	0.05	12-14
10	5	20	14	0.005	12-14
11	20	70	5.14	0.005	16b
12	50	30	29.3	-	16c

Table 2.   Properties held constant.

Parameter	Definition	Value	Units
K_x/K_y	anisotropy	100	dimensionless
D_d	solute diffusion coefficient	10^{-5}	$m^2 day^{-1}$
	top slope	0.005	dimensionless
	fore slope	0.05	dimensionless
	toe velocity	0.04	$mday^{-1}$
S_s	specific storage	10^{-3}	m^{-1}
Δt	time step size	100	Days
α_T	transverse dispersivity	$0.1\alpha_L$	m

that a normalized concentration of 1 is equivalent to seawater and has a fluid density of
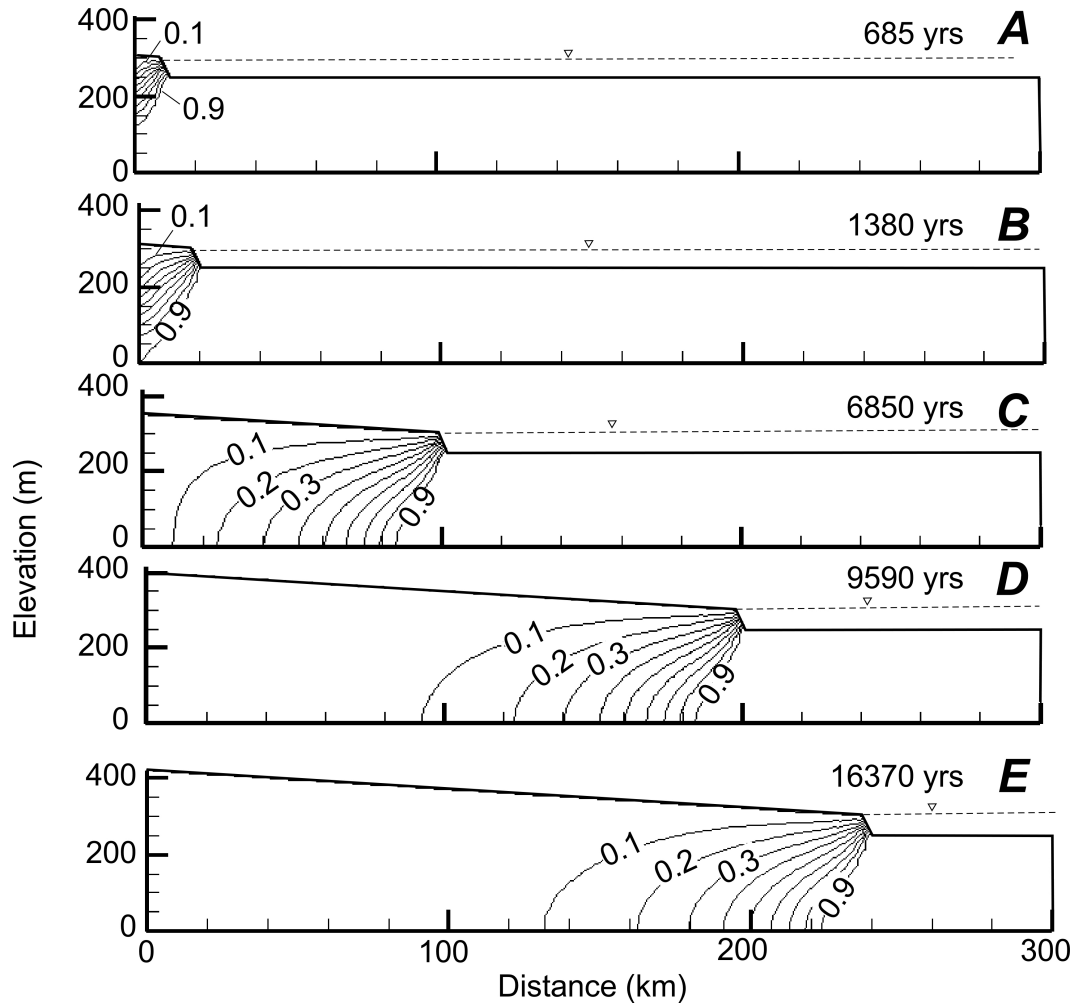1025 kg/m3.

Figure 7. Salinity evolution through time during shoreline progradation for the base case.

During early times, onshore freshwater propagates downward towards the bottom
of the model domain (Fig. 7a-7b). This is because connate seawater must first be dis-
placed by freshwater before lateral flushing can take place. During this time period, there
are significant changes in the magnitude of groundwater flux vertically (Fig. 8a-8c). The
lateral migration of the solute front is negligible. Once the toe of the freshwater-saltwater
mixing zone attaches to the bottom of the domain (Fig. 7c-7e) it migrates laterally, lag-
ging behind the shoreline toe. At early times, fluxes are highest near the land surface.

Longitudinal and transverse dispersivities strongly influences the downward rate
of propagation of the solute front. The lower the dispersitivy, the longer it takes for the
freshwater to reach the base of the model domain and begins to migrate laterally. The
final distribution of salinity at the end of each model run is shown in Figure 9 for lon-
gitudinal dispersivities between 50m to 20m. Recall that transverse dispersivities are set
to be an order of magnitude lower (Table 2). More seawater is "trapped" on shore be-
cause of the higher lag times for the freshwater interface to reach the base of the model
domain with lower dispersivities. The relative positions of the shoreline toe and the toe
of the freshwater-seawater mixing zone (normalized concentration of 0.05) through time
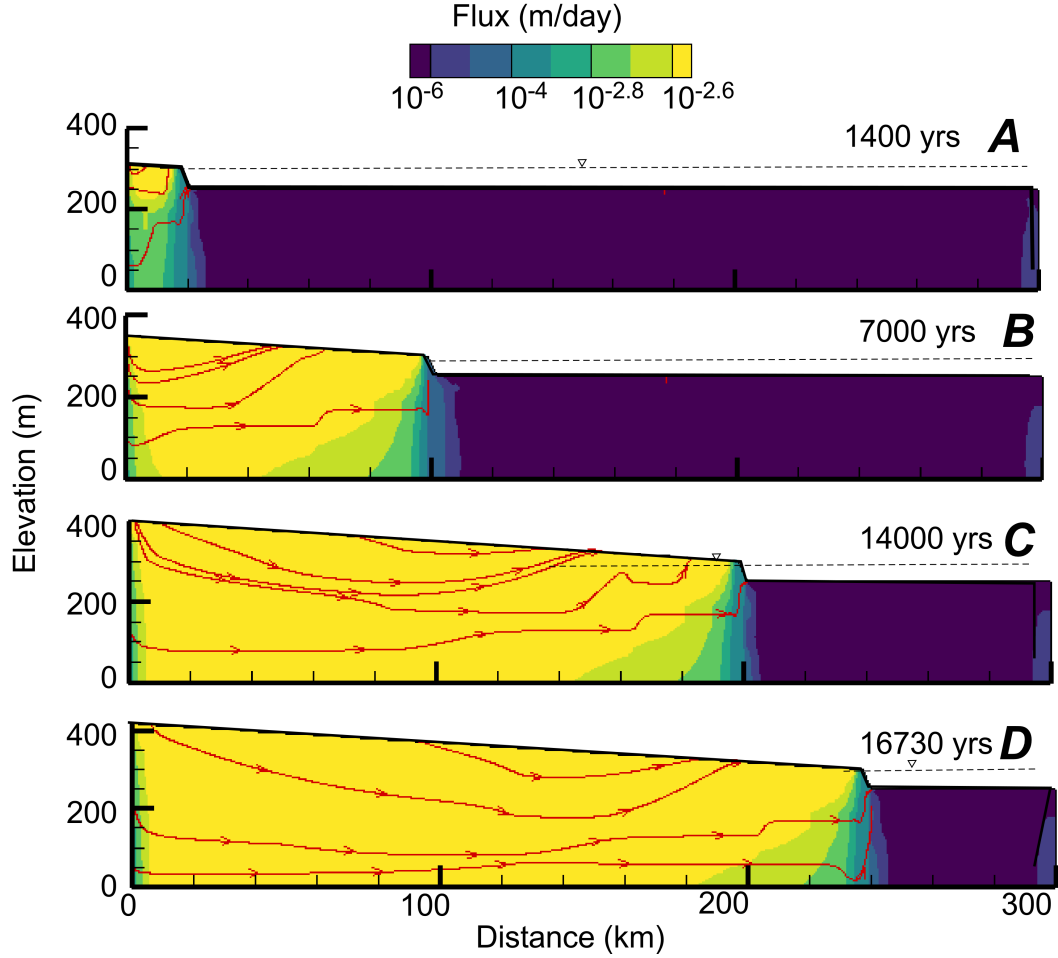
Figure 8. Groundwater flux evolution during shoreline progradation for the base case model run.

for the dispersivity model runs 1, 5-8 are shown in Figure 10. The toe of the interface lines do not begin at time equal zero because the freshwater toe has not reached the bottom the interface at early time is near the upper boundary. The portions of these lines that have curvature represent early time behavior when the freshwater-saltwater mixing zone is just reaching the base of the solution domain. Linear behavior occurs when the magnitude of the lateral velocity field becomes stationary. For the lowest dispersivity ($\alpha_L = 10$m), the lateral velocity field is never reached.

Changes in hydraulic conductivity also influences the rate of lateral propagation of the solute front (Figure 11). Higher hydraulic conductivity results in a linear increase in groundwater flow rates because the onshore water table slope is fixed at the land surface elevation. The higher the groundwater flow rates, the closer the freshwater-seawater mixing zone is to the shoreline. This can also be seen by plotting the relative positions of the shore line and mixing zone toes (Figure 12). The distances between the mixing zone position and the shoreline appear to be unchanged during basin evolution.

We conclude our sensitivity study by considering the presence of a discontinuous confining unit on trapping seawater onshore. The onshore hydrogeology of Bangladesh (Bengal delta) has both confined and unconfined aquifers separated by discontinuous clay
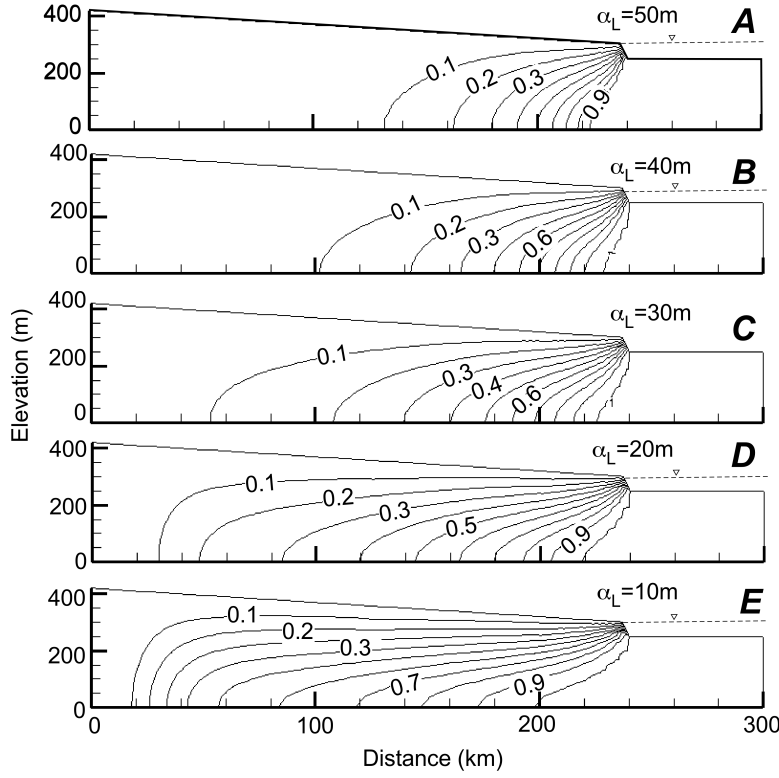
Figure 9. Effect of longitudinal dispersivity on salinity distribution. Parameters are listed in Table 1. Simulation results are at 16,370 years.
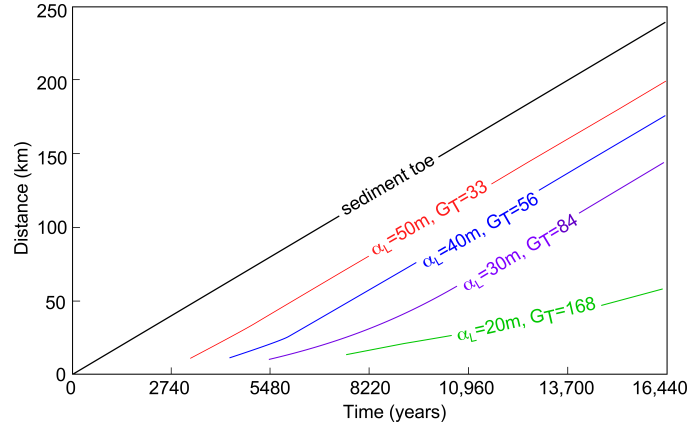

Figure 10. Computed toe of the shoreline (black line) and the toe of the saltwater-freshwater interface (c=0.05) and for the dispersivity simulations shown in Figure 8. The values of longitudinal dispersivity and the dimensionless number GT are listed with each line.
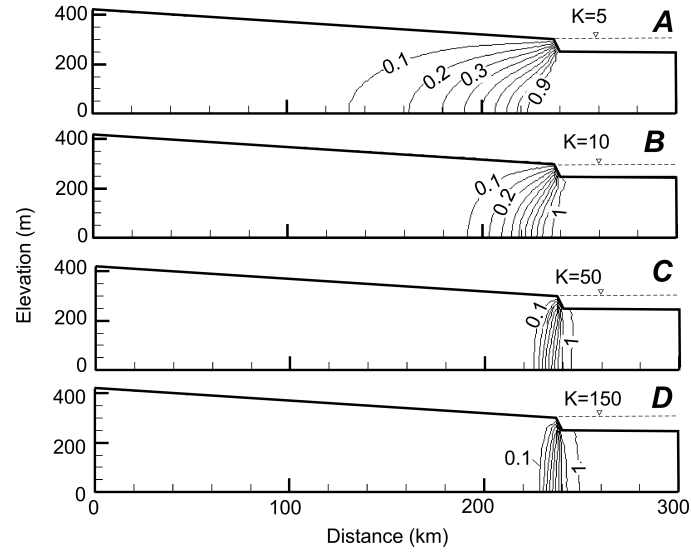
Figure 11. Effect of Hydraulic conductivity on salinity distribution. Parameters are listed in Table 1. Longitudinal dispersivity (aL) is fixed at 50m. Simulation results are at 16,370 years.
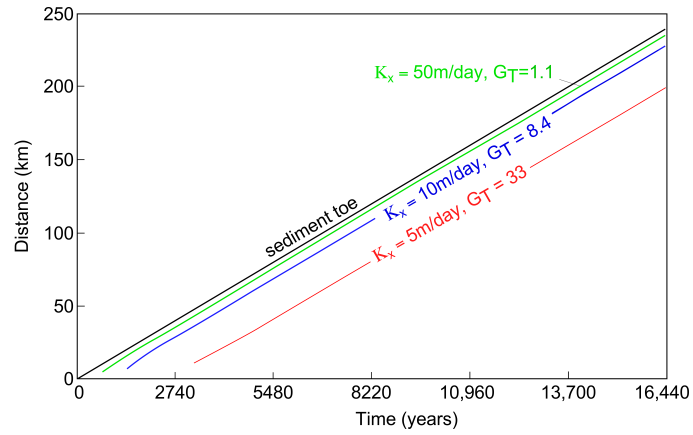

Figure 12. Changes in the position of the shoreline toe (black line) and the toe of the freshwater-saltwater interface (0.05 isochlor) during progradation. Colored lines represent changes in Hydraulic conductivity of 5 m/day, The numbers list the value of G_T.
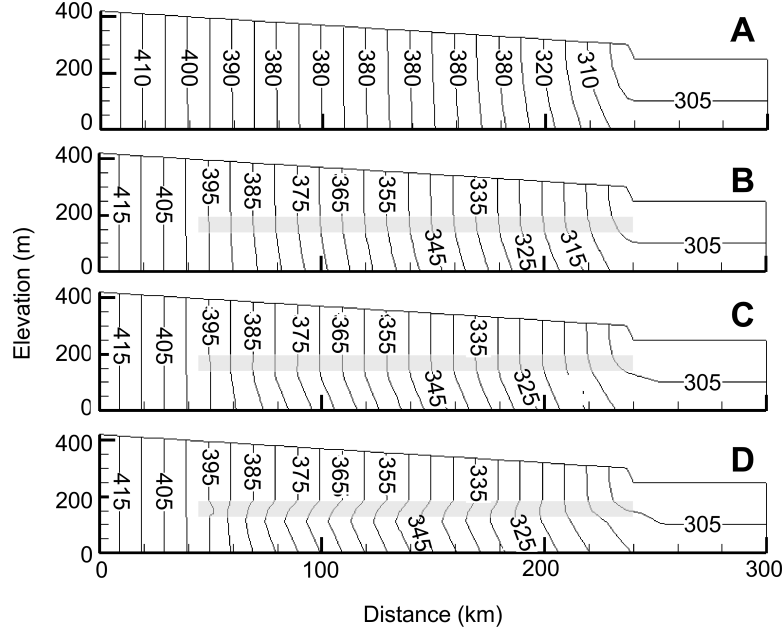
Figure 13. Contour maps of computed heads assuming an aquifer hydraulic conductivity of 5 m/day (K_{aq}) and (A) no confining unit. (B) Confining unit hydraulic conductivity is equal to $K_{aq}/10$. (C) Confining unit hydraulic conductivity is equal to $K_{aq}/100$. (D) Confining unit hydraulic conductivity is equal to $K_{aq}/1000$. The gray rectangle denotes the position of the confining layer. Simulation results are at 16,370 years.

and silt units (Goodbred Jr et al., 2003; Hoque et al., 2014). Figure 13 presents computed freshwater heads at the end of the simulation period for the base case (i.e., no confining unit) and for three other model runs (8-10) that include a confining unit whose hydraulic conductivity decreases by a factor of between 10 (Figure 13b), 100 (Figure 13c), and 1000 (Figure 13d). The aquifer hydraulic conductivity is fixed at 5m/day. In the absence of a confining unit, the head contours are nearly vertical indicating the dominance of horizontal flow (Figure 13a). As the confining hydraulic conductivity decreases, the head contours bend to a sub-horizontal configuration creating a higher component of vertical flow (Freeze & Witherspoon, 1967). As confining unit hydraulic conductivity decreased, there as a more entrapment of onshore seawater in the confined aquifer (Figure 14). Groundwater fluxes are nearly constant across and horizontal within the water table aquifer. Within the semi-confined aquifer, there is a progressive decrease in flux magnitude on the shoreward side of the system (Figure 15). For the lower conductivity confining unit scenarios, remnant seawater also lingers in in the confining unit near the shoreline. The magnitude of flux in the confined aquifer varies across the confining unit and decreases towards the shore but more slowly than in the overlying confined aquifer (Figure 15).

4 Discussion

Coastal aquifers in rapidly prograding deltas around the world are observed to have saline water tens of kilometers inland (Howard & Lloyd, 1983; Manzano et al., 2001; Custodio, 2010; Van Weert et al., 2009; Ravenscroft & McArthur, 2004; Shamsudduha, 2013). We argue here that brackish to saline water entrapped onshore can be the result of rapid progradation of the shoreline.
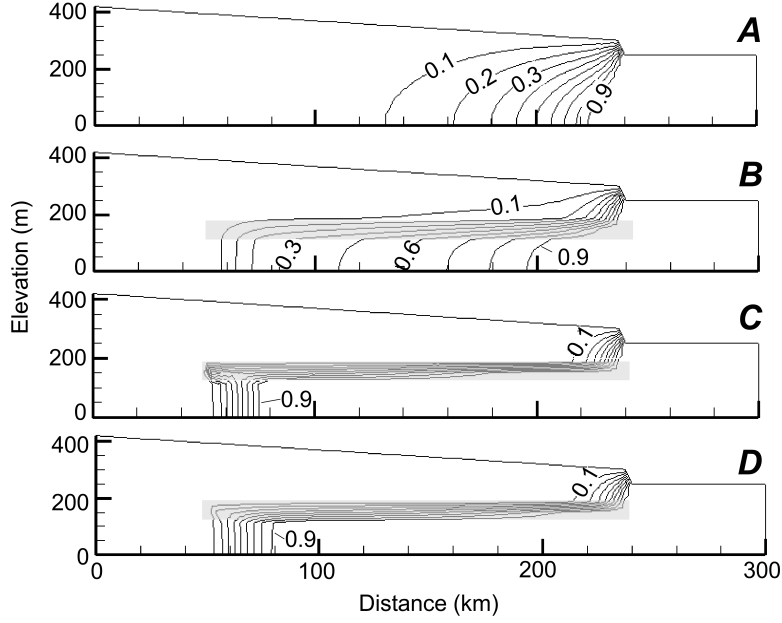
Figure 14. Effect of confining unit salinity on salinity patterns. Aquifer hydraulic conductivity 5 m/day (K_{aq}). (A) No confining unit. (B) Confining unit hydraulic conductivity is equal to $K_{aq}/10$. (C) Confining unit hydraulic conductivity is equal to $K_{aq}/100$. (D) Confining unit hydraulic conductivity is equal to $K_{aq}/1000$. The gray rectangle denotes the position of the confining layer. Simulation results are at 16,370 years.
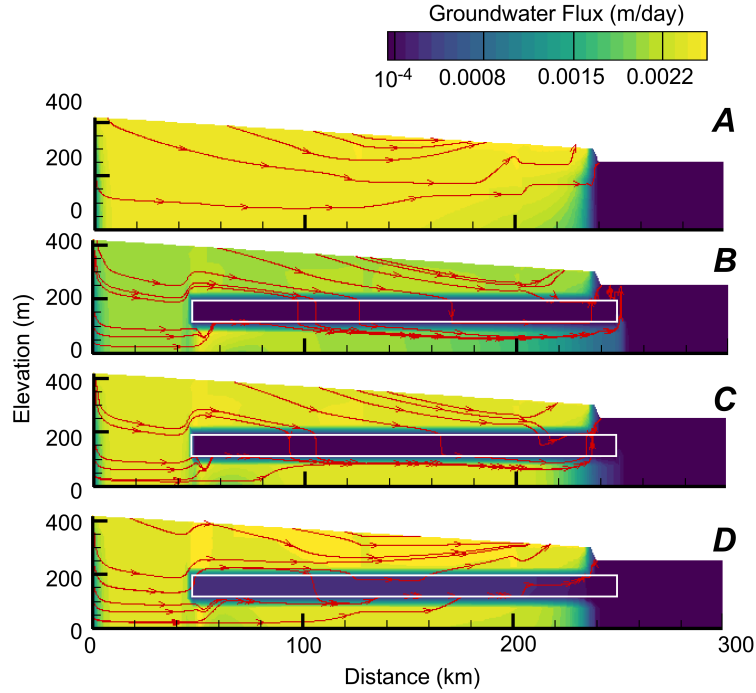

Figure 15. Contour maps of computed flux for the base case with no confining unit (A). (B) Confining unit hydraulic conductivity is equal to $K_{aq}/10$. (C) Confining unit hydraulic conductivity is equal to $K_{aq}/100$. (D) Confining unit hydraulic conductivity is equal to $K_{aq}/1000$. The white rectangle denotes the position of the confining layer. Simulation results are at 16,370 years.

Table 3. Global delta progradation rates over the Holocene

River	Country	Progradation Rate (m/yr)	Source
Ganges-Brahmaputra	Bangladesh	15-20	(Kuehl et al., 2005)
Mississippi	USA	100-150	(Chamberlain et al., 2018)
Pearl	China	29	(Zong et al., 2009)
Mekong	Vietnam	19-20	(Tanabe et al., 2003)
Mekong	Vietnam	50	(Zoccarato et al., 2018)
Yangtze	China	80	(Hori et al., 2001)
Amazon	Brazil	1-10	(Nittrouer et al., 1996)

The coupled sediment transport-coastal hydrogeologic model developed as part of this study reveals that inland seawater is the result of rapid progradation of the shoreline ($\sim 10 m/yr$). The distance that saline to brackish water is trapped onshore is sensitive to both aquifer hydraulic conductivity and solute dispersivity; in homogeneous aquifers there is an indication that trends follow the dimensionless group G_T defined in eq.(15). The presence of a confining unit, however, probably has the greatest impact in sequestering onshore seawater. Our results show that, even a contrast in aquifer/confining unit permeability of one order of magnitude, can trap significant amounts of seawater onshore.

We ran two additional simulations to provide field support for the concept that rapid progradation can entrap seawater on shore. The "best-fit" parameters used in these simulations are listed in Table 3 for the Bengal Delta (Run 11) and Mississippi River Delta (Run 12). We modified the geometry of the model domain and hydrogeology of the Mississippi River and Bengal Deltas to approximate field conditions. For the Bengal Delta model run, we only considered the unconfined and uppermost confined aquifers. The base of the Bengal Delta model was assumed to be the top of a tight confining unit. The Mississippi River Delta model only considered the unconfined aquifer system because our observational data only extended that deep (Stanton et al., 2017). We set the progradation rates equal to those reported in Table 3 for these two venues. We projected observed salinity data onto these idealized cross sections for comparison purposes (Figure 16a and 16d). There was general agreement between the computed and observed salinity conditions within the Bengal (Figure 16b) and Mississippi River (Figure 16e) Deltas. The present-day computed salinity conditions for a static grids (i.e., no progradation) are presented in Figures 16c and 16f for comparison purposes. As can be seen, sediment progradation dramatically modifies computed onshore salinity conditions. These model runs are not intended to represent calibrated models for the Mississippi River or Bengal Deltas. Rather, they are intended to illustrate that proof of concept that sediment progradation can play an important role in entrapping onshore seawater.

In all model runs, we have assumed sea-level was static when in fact, it rose by about 25m during the Holocene. Since the onshore topography increases due to progradation between 60m-140m, we feel this simplifying assumption is justified.

Observations of seawater entrapment could be improved by running controlled source electromagnetic surveys along inland river channels. These electromagnetic surveys would help fill in the gaps of sparse well data. Land based time domain electromagnetic or magnetotelluric soundings would also be useful though more time consuming.
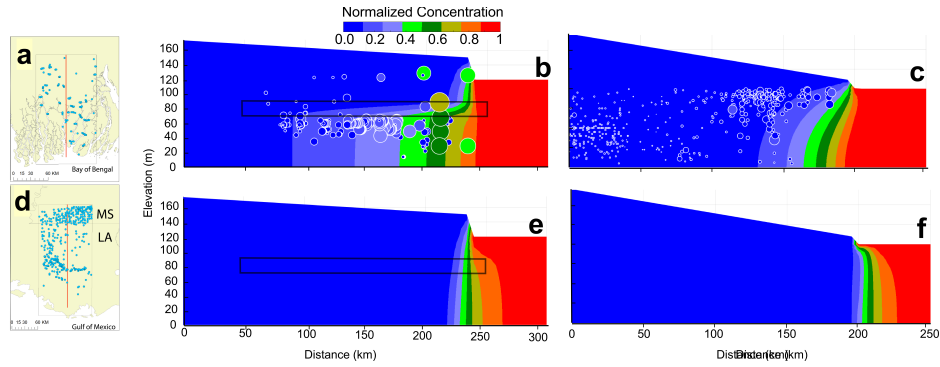
Figure 16. Location of Bengal Delta (a) and Mississippi River Delta (d) cross sections onto which salinity data was interpolated. Best fit model simulation results at the present day are shown in 16b and 16c for the Bengal Delta and Mississippi River Delta. Computed salinity levels using the same parameters using a static grid (no progradation) for the Bengal Delta and Mississippi River Delta venues are presented in (e) and (f) respectively. Parameters used in these model runs are presented in Table 1. Parameters in Runs 11 and 12 in Table 1 refer to the Bengal and Mississippi River Deltas, respectively. The colored circles represent normalized salinity conditions. A salinity level of 1.0 is seawater salinity conditions. The circle size also reflects salinity levels.

5 Conclusions

In this study, we have developed a coupled sediment transport -coastal hydrogeologic model using the control volume finite element method. The code was verified using the Henry solution (Fahs et al., 2016). The code included a novel mesh generation algorithm to take into account sediment deposition and shoreline progradation. We found that the entrapment of seawater onshore can be described by the product of two dimensionless number groups (eq. 15). One is the ratio of the sediment (shoreline) toe and groundwater velocities (eq. 13). The other dimensionless number group is the Peclet number (eq. 14).

We conducted a sensitivity study in which we varied sediment hydraulic conductivity and dispersivity. Some simulations include a lower permeable, semi-confining unit. Assuming a lateral shoreline velocity of 14.6 m/yr, we found that an aquifer hydraulic conductivity of less than 10m/day and a longitudinal dispersivity of less than 50m could sequester onshore seawater. The presence of a confining unit had the largest impact on onshore seawater entrapment. Conducting towed electromagnetic surveys along inland rivers and onshore in undeveloped delta regions will help to better constrain the distribution of onshore seawater.

References

Barlow, P. M., & Reichard, E. G. (2010, February). Saltwater intrusion in coastal regions of North America. *Hydrogeology Journal*, *18*(1), 247–260. doi: 10.1007/s10040-009-0514-3

Bear, J. (1972). *Dynamics of Fluids in Porous Media*. Amsterdam, Holland: Elsevier.

BWDB. (2013). *Hydrogeological study and mathematical modelling to identify sites for installation of observation well nests, selection on model boundary, supervision of pumping test, slug test, assessment of different hydrologeological parameters collection and conduct chemical analysis of surface water and groundwater, final report (main volume, package 3)* (Tech. Rep.). Bangladesh Water Development Board.

Chamberlain, E. L., Törnqvist, T. E., Shen, Z., Mauz, B., & Wallinga, J. (2018). Anatomy of Mississippi Delta growth and its implications for coastal restoration. *Science Advances*, *4*(4).

Chui, T. F. M., & Terry, J. P. (2013, October). Influence of sea-level rise on freshwater lenses of different atoll island sizes and lens resilience to storm-induced salinization. *Journal of Hydrology*, *502*, 18–26. doi: 10.1016/j.jhydrol.2013.08.013

Custodio, E. (2010). Coastal aquifers of Europe: an overview. *Hydrogeology Journal*, 12.

Fahs, M., Ataie-Ashtiani, B., Younes, A., Simmons, C. T., & Ackerer, P. (2016). The Henry problem: New semianalytical solution for velocity-dependent dispersion. *Water Resour. Res.*, *52*, 7382–7407. doi: 10.1002/2016WR019288

Freeze, R. A., & Witherspoon, P. A. (1967). Theoretical analysis of regional groundwater flow: 2. Effect of water-table configuration and subsurface permeability variation. *Water Resources Research*, *3*(2), 623–634. doi: 10.1029/WR003i002p00623

Goodbred Jr, S. L., Kuehl, S. A., Steckler, M. S., & Sarker, M. H. (2003). Controls on facies distribution and stratigraphic preservation in the ganges–brahmaputra delta sequence. *Sedimentary Geology*, *155*(3-4), 301–316.

Han, D., Post, V. E., & Song, X. (2015, December). Groundwater salinization processes and reversibility of seawater intrusion in coastal carbonate aquifers. *Journal of Hydrology*, *531*, 1067–1080. doi: 10.1016/j.jhydrol.2015.11.013

Hoque, M. A., McArthur, J. M., & Sikdar, P. K. (2014). Sources of low-arsenic groundwater in the Bengal Basin: Investigating the influence of the last glacial maximum palaeosol using a 115-km traverse across Bangladesh. *Hydrogeology Journal*, *22*, 1535–1547. doi: 10.1007/s10040-014-1139-8

Hori, K., Saito, Y., Zhao, Q., Cheng, X., Wang, P., Sato, Y., & Li, C. (2001, November). Sedimentary facies and Holocene progradation rates of the Changjiang (Yangtze) delta, China. *Geomorphology*, *41*(2), 233–248. doi: 10.1016/S0169-555X(01)00119-2

Howard, K. W. F., & Lloyd, J. W. (1983). Major Ion Characterization of Coastal Saline Ground Waters. *Groundwater*, *21*(4), 429–437. doi: 10.1111/j.1745-6584.1983.tb00744.x

K.G. Villholth, & Neupane, B. (2011). Tsunamis as long-term hazards to coastal groundwater resources and associated water supplies. *Tsunami-A growing disaster*, 87–104.

Kim, W., Paola, C., Swenson, J. B., & Voller, V. R. (2006). Shoreline response to autogenic processes of sediment storage and release in the fluvial system. *Journal of Geophysical Research: Earth Surface*, *111*(F4). doi: 10.1029/2006JF000470

Kuehl, S., Allison, M., Goodbred, S., & Kudrass, H. (2005, January). The Ganges–Brahmaputra Delta. In *River Deltas - Concepts, Models and Examples*

(Vol. 83, pp. 413–434). doi: 10.2110/pec.05.83.0413

Lee, S., Currell, M., & Cendón, D. I. (2016, February). Marine water from mid-Holocene sea level highstand trapped in a coastal aquifer: Evidence from groundwater isotopes, and environmental significance. *Science of The Total Environment*, *544*, 995–1007. doi: 10.1016/j.scitotenv.2015.12.014

Lorenzo-Trueba, J., Voller, V. R., Muto, T., Kim, W., Paola, C., & Swenson, J. B. (2009). A similarity solution for a dual moving boundary problem associated with a coastal-plain depositional system. *J. Fluid Mech.*, *628*, 427–443. doi: 10.1017/S0022112009006715

Manzano, M., Custodio, E., Loosli, H., Cabrera, M. C., Riera, X., & Custodio, J. (2001, January). Palaeowater in coastal aquifers of Spain. *Geological Society, London, Special Publications*, *189*(1), 107–138. doi: 10.1144/GSL.SP.2001.189.01.08

Nittrouer, C. A., Kuehl, S. A., Figueiredo, A. G., Allison, M. A., Sommerfield, C. K., Rine, J. M., . . . Silveira, O. M. (1996, January). The geological record preserved by Amazon shelf sedimentation. *Continental Shelf Research*, *16*(5), 817–841. doi: 10.1016/0278-4343(95)00053-4

Patankar, S. V. (1980). *Numerical Heat Transfer and Fluid Flow*. Washington, USA: Hemisphere.

Pauw, P., de Louw, P., & Essink, G. O. (2012, November). Groundwater salinisation in the Wadden Sea area of the Netherlands: quantifying the effects of climate change, sea-level rise and anthropogenic interferences. *Netherlands Journal of Geosciences - Geologie en Mijnbouw*, *91*(3), 373–383. doi: 10.1017/S0016774600000500

Post, V., Kooi, H., & Simmons, C. (2007). Using hydraulic head measurements in variable-density ground water flow analyses. *Groundwater*, *45*(6), 664–671.

Ravenscroft, P., & McArthur, J. M. (2004, September). Mechanism of regional enrichment of groundwater by boron: the examples of Bangladesh and Michigan, USA. *Applied Geochemistry*, *19*(9), 1413–1430. doi: 10.1016/j.apgeochem.2003.10.014

Reynolds, D. J., Steckler, M. S., & Coakley, B. J. (1991). The role of the sediment load in sequence stratigraphy: The influence of flexural isostasy and compaction. *J. Geophys. Res*, *96*, 6931–6949.

Shamsudduha, M. (2013). Groundwater-fed irrigation and drinking water supply in Bangladesh: challenges and opportunities. *Adaptation to the Impact of Climate Change on Socio-economic Conditions of Bangladesh. Dhaka: Alumni Association of German Universities in Bangladesh, German Academic Exchange Service (DAAD)*.

Stanton, J. S., Anning, D. W., Brown, C. J., Moore, R. B., McGuire, V. L., Qi, S. L., . . . others (2017). *Brackish groundwater in the united states* (Tech. Rep.). US Geological Survey.

Tanabe, S., Ta, T. K. O., Nguyen, V. L., Tateishi, M., Kobayashi, I., & Saito, Y. (2003). Delta Evolution Model Inferred From the Holocene Mekong Delta, Southern Vietnam. *Special Publications of SEPM*.

Van Weert, F., Van der Gun, J., & Reckman, J. (2009). Global overview of saline groundwater occurrence and genesis. *International Groundwater Resources Assessment Centre*.

Violette, S., Boulicot, G., & Gorelick, S. M. (2009, April). Tsunami-induced groundwater salinization in southeastern India. *Comptes Rendus Geoscience*, *341*(4), 339–346. doi: 10.1016/j.crte.2008.11.013

Voller, V. R. (2009). *Basic Control Volume Finite Element Methods for Fluids and Solids*. Singapore: World Scientific.

Voller, V. R., Swenson, J. B., & Paola, C. (2020). The thin blue line: A review of shoreline dynamics across time scales and environments. *Earth Surf. Process. Landforms*, *45*, 96–108. doi: 10.1002/esp.4705

Zienkiewicz, O. C., Taylor, R. L., & Zhu, J. Z. (2005). *The Finite Element Method: it's Basics and Fundamentals* (6th ed.). Amsterdam, Holland: Elsevier.

Zoccarato, C., Minderhoud, P. S. J., & Teatini, P. (2018, July). The role of sedimentation and natural compaction in a prograding delta: insights from the mega Mekong delta, Vietnam. *Scientific Reports*, *8*(1). doi: 10.1038/s41598-018-29734-7

Zong, Y., Huang, G., Switzer, A. D., Yu, F., & Yim, W.-S. (2009). An evolutionary model for the Holocene formation of the Pearl River delta, China. *The Holocene*, *19*(1).